

Phase-sensitive evidence for $d_{x^2-y^2}$ - pairing symmetry in the parent-structure high- T_c cuprate superconductor $\text{Sr}_{1-x}\text{La}_x\text{CuO}_2$

J. Tomaschko,¹ S. Scharinger,¹ V. Leca,^{1,2} J. Nagel,¹ M. Kemmler,¹ T. Selistrovski,¹ D. Koelle,¹ and R. Kleiner^{1,*}

¹Physikalisches Institut – Experimentalphysik II and Center for Collective Quantum Phenomena in LISA⁺, Universität Tübingen, Auf der Morgenstelle 14, 72076 Tübingen, Germany

²National Institute for Research and Development in Microtechnologies, Molecular Nanotechnology Laboratory, Erou Iancu Nicolae Str. 126A, RO-077190, Bucharest, Romania

(Dated: September 23, 2018)

Even after 25 years of research the pairing mechanism and – at least for electron doped compounds – also the order parameter symmetry of the high transition temperature (high- T_c) cuprate superconductors is still under debate. One of the reasons is the complex crystal structure of most of these materials. An exception are the infinite layer (IL) compounds consisting essentially of CuO_2 planes. Unfortunately, these materials are difficult to grow and, thus, there are only few experimental investigations. Recently, we succeeded in depositing high quality films of the electron doped IL compound $\text{Sr}_{1-x}\text{La}_x\text{CuO}_2$ (SLCO), with $x \approx 0.15$, and on the fabrication of well-defined grain boundary Josephson junctions (GBJs) based on such SLCO films. Here we report on a phase sensitive study of the superconducting order parameter based on GBJ SQUIDs from a SLCO film grown on a tetracystal substrate. Our results show that also the parent structure of the high- T_c cuprates has $d_{x^2-y^2}$ -wave symmetry, which thus seems to be inherent to cuprate superconductivity.

PACS numbers: 74.50.+r, 74.72.-h, 74.72.Ek, 85.25.Dq

Since the discovery of high transition temperature (high- T_c) superconductivity in cuprates¹, tremendous work has been performed on these materials. Researchers succeeded in increasing T_c from initially 30 K to 135 K^{2–4} by synthesizing increasingly complex compounds. However, the microscopic mechanism causing high- T_c superconductivity still has not been identified and is one of the biggest issues in solid state physics. All these materials have in common that superconductivity resides in the copper oxide (CuO_2) planes where superconducting charge carriers, Cooper pairs, form. An “infinite layer” (IL) cuprate consisting essentially of CuO_2 planes is therefore of fundamental interest for all questions addressing the basics of high- T_c superconductivity. In 1988, Siegrist *et al.* succeeded in synthesizing such a simple cuprate, which is known as the “parent structure” of cuprate superconductors⁵. Its CuO_2 planes are only separated by a single alkaline earth metal plane ($A = \text{Ca}, \text{Sr}$ or Ba), forming a $AC\text{uO}_2$ crystal. Upon electron-doping, it turned out to be superconducting with maximum $T_c = 43$ K^{6–9}.

A striking and highly debated feature of the cuprate superconductors is their unconventional order parameter symmetry. Whereas for hole-doped cuprates $d_{x^2-y^2}$ -wave pairing has been established^{10–12}, for electron-doped cuprates¹³ the issue is not yet completely settled. After controversial discussion, the electron-doped T' -compounds $L_{2-x}\text{Ce}_x\text{CuO}_4$ ($L = \text{La}, \text{Pr}, \text{Nd}, \text{Eu}$ or Sm) have been shown to be predominant $d_{x^2-y^2}$ -wave superconductors by a number of phase-sensitive experiments^{14–17}. By contrast, for the parent compounds the pairing symmetry is essentially still unknown, since a variety of experimental tests yielded conflicting results^{13,18–27}. Phase-sensitive tests, such as experiments on corner junctions²⁸, tricrystal rings²⁹ or tetracrys-

tal SQUIDs^{15,30,31}, are widely recognized to provide a clear evidence for the pairing symmetry of the order parameter¹². Such experiments rely on Josephson junctions, which for IL cuprate thin films became available only very recently³².

Here we report on the fabrication and characterization of thin-film $\text{Sr}_{1-x}\text{La}_x\text{CuO}_2$ (SLCO) dc SQUIDs based on BaTiO_3 -buffered tetracystal SrTiO_3 substrates. The geometry involved is designed to be frustrated for $d_{x^2-y^2}$ -wave pairing, i.e. the SQUID ring comprising the tetracystal point contains one 0 junction and one π junction, if the order parameter has $d_{x^2-y^2}$ -wave symmetry. This device will be referred to as π -design SQUID. Its geometry, together with the design of a reference SQUID, is sketched in Fig. 1. There are four grain boundaries (GBs), labelled 1–4. GBs 1–3 have misorientation angles of 30°, while the misorientation angle of GB 4 is 0°. The π -design SQUID comprises all GBs. GB 4 will not form a grain boundary junction (GBJ) due to its 0° misalignment angle, in contrast to GBs 1–3. GBs 2 and 3, having a width of 58 μm , form the active Josephson junctions in the current and voltage lead configuration indicated in Fig. 1. The bias current also passes GBJ 1 which, however, is much longer (~ 1.5 mm) than GBJs 2 and 3 and thus will have a much higher critical current. Below, we will see however, that flux quanta (Josephson fluxons) can enter this GBJ, which thus cannot be ignored in the data analysis. If SLCO is a $d_{x^2-y^2}$ -wave superconductor, one of GBJs 2 and 3 faces a sign change of the order parameter (GBJ 3 in Fig. 1), thus forming a π Josephson junction. The other GBJs are conventional. The area of GBJs 2 and 3 is not much smaller than the area of the SQUID hole. In this “spatially distributed junction” design³³ the junction’s I_c vs. H modulation (Fraunhofer pattern) is superposed on the SQUID mod-

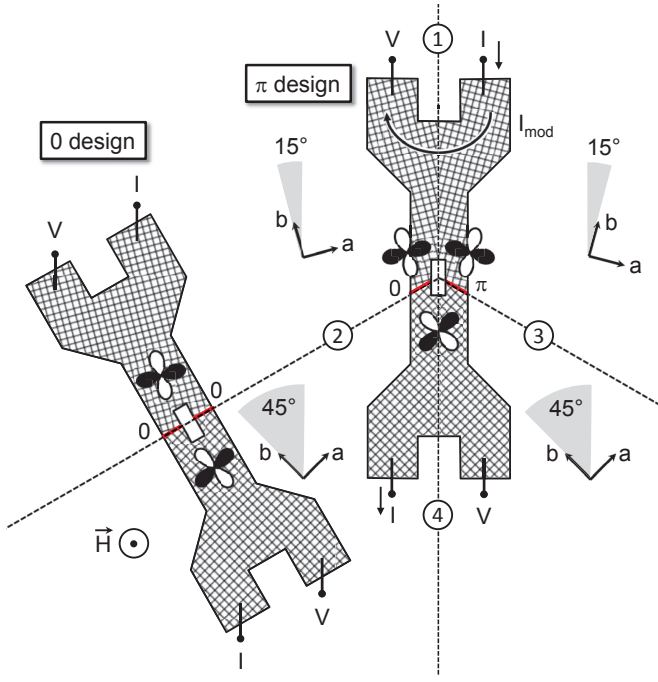


FIG. 1: (Color online) Schematic layout of the SQUIDs. The 0-design SQUID comprises two conventional GBJs (0 junctions) straddling a single 30° [001]-tilt grain boundary. The π -design SQUID comprises four GBs. The misorientation angle of GB 4 is 0° . All other misorientation angles are 30° . The $d_{x^2-y^2}$ -wave order parameter is indicated by the clover-leaf structure consisting of white and black lobes, indicating the sign change of the order parameter. Leads for bias current I and voltage V are indicated. In some experiments, for the π -design SQUID we have also sent a current I_{mod} across GB 1. Magnetic fields have been applied perpendicular to the substrate plane.

ulation on a similar field scale. The (a)symmetry of the SQUID modulation relative to the Fraunhofer envelope allows to detect residual fields and often also trapped magnetic flux.

The reference SQUIDs – there were two reference SQUIDs, producing very similar results – cross only one of the 30° GBs and incorporate two $50\ \mu\text{m}$ wide GBJs, which act as conventional junctions both for s-wave and $d_{x^2-y^2}$ -wave order parameters. Below, these devices will be referred to as the 0-design SQUIDs. Both the π -design SQUID and the reference SQUIDs had rectangular SQUID holes with an area $A_S = 50 \times 75\ \mu\text{m}^2$.

The samples have been fabricated by pulsed laser deposition, as described elsewhere^{32,34,35}. In brief, we first deposited a $25\ \text{nm}$ thick BaTiO_3 thin-film on the SrTiO_3 tetracystal, acting as a buffer layer. This layer was followed by a $22\ \text{nm}$ thick SLCO thin-film, with doping $x \approx 0.15$. Finally, a $10\ \text{nm}$ thick gold layer was evaporated in-situ, protecting SLCO from degradation and acting as resistive shunt for the GBJs. The SQUIDs were patterned by standard photolithography and argon

ion milling. The SLCO film had a critical temperature $T_c \approx 18\ \text{K}$. Electric transport measurements were performed at $T = 4.2\ \text{K}$ in a four-point configuration, with the sample mounted inside a noise-filtered, magnetically and radio frequency shielded probe in a liquid-helium dewar. A SQUID amplifier was used to allow for low-noise measurements.

Below we discuss data of one of the 0-design SQUIDs and of the π -design SQUID. The current voltage (IV) characteristics of these devices were nonhysteretic and could be well reproduced by the SQUID Langevin equations, extended by taking the nonzero junction width into account. Details can be found in Ref. 36, giving reasonable values for the junction parameters I_0 (maximum amplitude of Josephson current), R (junction resistance) and C (junction capacitance). The junctions of each device were symmetric in terms of I_0 , R and C , with values $I_0 = 8.2\ \mu\text{A}$, $R = 0.92\ \Omega$, $C = 24\ \text{pF}$ (0-design SQUID) and $I_0 = 12.2\ \mu\text{A}$, $R = 0.87\ \Omega$, $C = 25\ \text{pF}$ (π -design SQUID). For the inductance parameter $\beta_L = 2I_0L/\Phi_0$, where Φ_0 is the magnetic flux quantum and L is the total inductance of the SQUID, we found $\beta_L = 1.4$ (0-design SQUID; $L = 177\ \text{pH}$) and 2.2 (π -design SQUID; $L = 187\ \text{pH}$), with an asymmetry $a_L = 0.05$ between the left and right arm of the SQUID (both designs). A fraction $f_J = 0.128$ (0-design SQUID) and $f_J = 0.12$ (π -design SQUID) of the flux Φ applied to the SQUID loop was coupled to each junction. The numbers for f_J were derived from an analysis of the SQUID critical current I_c vs. applied field H (see below).

Fig. 2 (a) shows the measured I_c vs. H for the 0-design SQUID (black line). I_c was determined using a voltage criterion $V_c = 50\ \text{nV}$. To identify magnetic hysteresis effects, I_c vs. H was traced from $2.8\ \mu\text{T}$ to $-2.8\ \mu\text{T}$ and back to $2.8\ \mu\text{T}$. One observes a SQUID modulation with period $\mu_0\Delta H = 0.175\ \mu\text{T}$ on top of a Fraunhofer-like modulation, which is due to the finite junction size. No hysteresis is visible. The modulation period corresponds to an effective SQUID area of $1.18 \cdot 10^4\ \mu\text{m}^2$, pointing to a flux compression of about 3.15. This is reasonable for our structures^{15,37}. The insets of Fig. 2 (a) show I_c vs. H near $H = 0$ for both positive and negative I_c . The I_c maximum is close to $H = 0$, with a small offset of $10.6\ \text{nT}$ for positive I_c and $5.2\ \text{nT}$ for negative I_c . We contribute the asymmetry of $\pm 2.7\ \text{nT}$ in offsets to an inductance asymmetry ($a_L = 0.05$) of the two SQUID arms and the average part of $7.9\ \text{nT}$ to residual fields in the cryostat. The red line in Fig. 2 (a) is a numerical calculation. It produces data very well inside the main maximum of the Fraunhofer envelope. The first Fraunhofer side-maximum is lower in amplitude than the experimental data, presumably due to a field distribution inside the junction, which is more complex than the homogeneous flux density assumed in our model. Most importantly, however, we see that the 0-design SQUID behaves as it should be expected from a conventional 0-SQUID.

The measured I_c vs. H of the π -design SQUID is shown by the black line in Fig. 2 (b). Also here we have

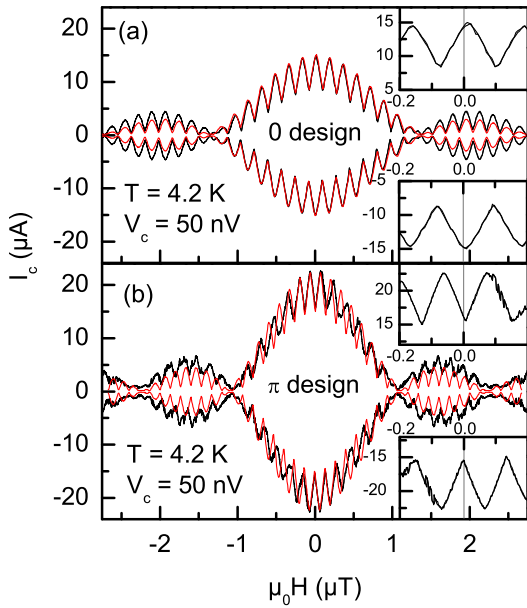


FIG. 2: (Color online) Critical current I_c vs. applied magnetic field H of (a) the 0-design SQUID and (b) the π -design SQUID (black lines) together with calculated curves (red lines) for (a) a 0 SQUID and (b) a π SQUID. Insets show I_c vs. H on expanded scales. A 50 nV voltage criterion was used to determine I_c .

varied H from $2.8 \mu\text{T}$ to $-2.8 \mu\text{T}$ and back to $2.8 \mu\text{T}$. I_c is at a *minimum* near $H = 0$ - a feature which appears when one of the two Josephson junctions *exhibits an additional π shift in its phase*. At negative I_c the minimum is at $\mu_0 H \approx 0.15 \text{nT}$, while at positive I_c it appears at $\mu_0 H \approx 7.8 \text{nT}$, pointing to an offset field of about 4nT and a small asymmetry in inductance ($a_L = 0.05$). The SQUID modulation period is $\mu_0 \Delta H = 0.136 \mu\text{T}$, corresponding to an effective area of $1.52 \cdot 10^4 \mu\text{m}^2$ and a flux compression factor of 4.05. The overall modulation of I_c vs. H is described reasonably well by numerical calculations (red line), however less well than I_c vs. H of the 0-design SQUID.

A prominent feature are the jumps in I_c , visible at $\mu_0 H > 89 \text{nT}$ at positive I_c and at $\mu_0 H < -80 \text{nT}$ at negative I_c . There is only a very tiny hysteresis associated with these jumps, which is not even visible in Fig. 2 (b). By comparing measured and calculated I_c vs. H curves within the main Fraunhofer lobe one sees that the calculated curve exhibits one additional SQUID period. These features indicate that magnetic flux quanta enter the device at each jump. This effect was not visible for the 0-design SQUID. A strong candidate for flux entry is thus GBJ 1 which is absent in the reference SQUID. Note that the I_c jumps visible in Fig. 2 (b) occur point-symmetric, *i.e.*, at positive I_c they occur at positive fields, while at negative I_c the field is negative, with about the same amplitude as for positive I_c . This feature can also clearly be seen in V vs. Φ patterns taken at many values of bias

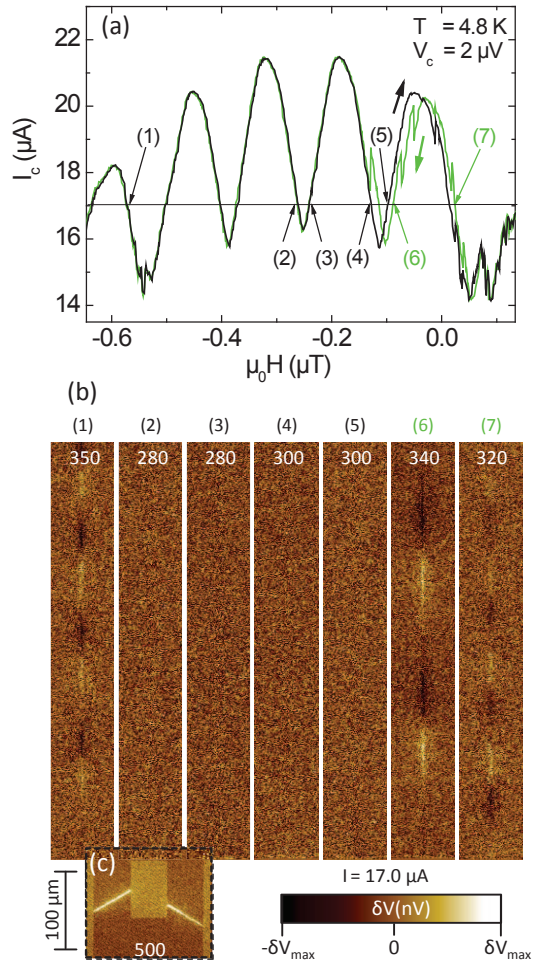


FIG. 3: (Color online) LTSEM data: (a) I_c vs. H , as measured in the LTSEM setup (black and green lines distinguish sweep directions), (b) δV images, taken along GBJ 1 at $I = 17 \mu\text{A}$ [horizontal line in (a)] at the magnetic field values (1) – (7) indicated in (a). Graph (c) shows a δV image of the SQUID hole and GBJs 2 and 3 at $I = 22 \mu\text{A}$ and $\mu_0 H = -0.19 \mu\text{T}$. This image has been superposed to scale to image (b)-(2) in order to indicate the position of the SQUID hole. For each image δV_{max} is indicated inside the graphs.

current, see Ref. 36. There we also show, that the point symmetry in I_c vs. H holds even for large values of H , and that applying an additional current I_{mod} across GBJ 1 alters the values of H in a way that is compatible with the notion of Josephson fluxons having entered GBJ 1.

For a final proof we have imaged the current distribution of the π -design SQUID using low temperature scanning electron microscopy (LTSEM). Details of the method can be found in Refs. 17,38. In brief, the pulsed electron beam, which is scanned across the sample, causes local heating by $\sim 1 \text{ K}$. The measured integral quantity is the voltage V across the SQUID, which is biased slightly above I_c . The electron beam causes a change $\delta V(x, y)$ depending on the beam position (x, y) . When the beam is scanned across GBJs 2 and 3 near a I_c maximum, a

positive signal appears, because I_c is lowered, causing a slight increase of V (cf. Fig. 3 (c)). When GBJ 1 is free of vortices no signal is expected from this GB. By contrast, when Josephson fluxons are present, local heating will alter the screening currents around the fluxons. In a heated area the Cooper pair density and thus the maximum supercurrent density is suppressed, causing an increase of the Josephson length λ_J and, thus, the fluxon is virtually deformed towards the heated area. When the electron beam is between the fluxon center and the SQUID hole this causes an increase of the fluxon's stray flux coupled to the SQUID and thus a change in I_c . In the opposite case the stray flux is decreased. A fluxon will thus appear as a bipolar signal $\delta V(x, y)$, with increased/decreased voltage relative to the unperturbed value of V . In a similar way, Abrikosov vortices trapped in a $\text{YBa}_2\text{Cu}_3\text{O}_7$ SQUID³⁸, as well as Josephson fluxons having entered a GBJ³⁹, have been imaged by LTSEM.

Fig. 3 (a) shows I_c vs. H , as measured in the LTSEM setup at $T = 4.8\text{ K}$ using a voltage criterion $V_c = 2\text{ }\mu\text{V}$. There is a stronger offset field ($\sim 0.25\text{ }\mu\text{T}$) than in the transport setup, causing a shift by about 2 SQUID modulation periods. Due to the Fraunhofer envelope this shift is straightforward to recognize. The two sweep directions of H have been distinguished by black and green lines. There is a nonhysteretic region around the offset field; at larger values of H , I_c jumps occur, leading to magnetic hysteresis. δV images of GBJ 1, cf. Fig. 3 (b), have been taken at $I = 17\text{ }\mu\text{A}$ at the field values indicated by labels (1)–(7) in Fig. 3 (a). No contrast appears when the sample is biased near the offset field [images (2), (3)] or at a field smoothly extending this I_c vs. H pattern [images (4),(5)]. By contrast, when I_c jumps have occurred, we observed a periodically modulated signal, having a period decreasing with the field amplitude H relative to the offset field [images (1),(6),(7)]. This is very indicative of Josephson fluxons having entered GBJ 1. In Fig. 3 (c) we also show a δV image of the area around the SQUID hole and GBJs 2 and 3. The image has been taken in a separate run, because we did not want to disturb the images of Fig. 3 (b) by scanning across these GBJs. It has been taken at the maximum of the SQUID modulation at $I = 22\text{ }\mu\text{A}$ and $\mu_0 H = -0.19\text{ }\mu\text{T}$. The image is superposed to scale to image Fig. 3 (b)-(2), to give an impression of the position of the SQUID hole and GBJs 2 and 3 relative to the images of Fig. 3 (b).

The LTSEM data clearly show that the I_c vs. H region of interest is free of trapped flux; we thus feel safe in interpreting the π -design data in favor of a $d_{x^2-y^2}$ -wave symmetry of $\text{Sr}_{1-x}\text{La}_x\text{CuO}_2$.

One may in addition ask about subdominant order parameters. A real superposition $d_{x^2-y^2}\pm s$ is not very likely due to the tetragonal crystal symmetry but, if present, could lead to an asymmetry of the critical currents of GBJs 2 and 3 and, in consequence, to a similar shift as the one we interpreted in terms of an inductance asymmetry. On the other hand, the 0-design SQUID should not show this asymmetry and we thus believe that an inductance asymmetry is more likely. By contrast, a complex admixture of a subdominant order parameter would lead to a ground state phase different from π or 0. Then, the SQUID modulation would shift relatively to the Fraunhofer envelope, making the amplitude of the inner I_c maxima asymmetric. This effect is not observed at least on a $\sim 5\%$ level.

In summary, our data clearly show, that the superconducting order parameter of the electron doped infinite-layer high- T_c cuprate $\text{Sr}_{1-x}\text{La}_x\text{CuO}_2$ has $d_{x^2-y^2}$ -wave symmetry. The phase sensitive configuration used was a π SQUID patterned on a tetracystal. The parasitic effect of Josephson fluxons entering one of the grain boundary junctions has been ruled out by direct imaging of the local supercurrent contribution. $\text{Sr}_{1-x}\text{La}_x\text{CuO}_2$ has the most simple crystal structure of all high- T_c cuprates. We conclude that the $d_{x^2-y^2}$ -wave symmetry is inherent to cuprate superconductivity and neither restricted to hole doping nor related to the complex crystal structures that complicates an analysis of almost all other cuprate superconductors.

Acknowledgments

J. T. gratefully acknowledges support by the Evangelisches Studienwerk e.V. Villigst and J. N. by the Carl-Zeiss Stiftung. V. L. acknowledges partial financial support by a grant of the Romanian National Authority for Scientific Research, CNCS UEFISCDI, project number PN-II-ID-PCE-2011-3-1065. This work was funded by the Deutsche Forschungsgemeinschaft (project KL 930/11).

* Electronic address: kleiner@uni-tuebingen.de

¹ J. G. Bednorz and K. A. Müller, *Z. Phys. B* **64**, 189 (1986).

² M.-S. Kim, M.-K. Bae, W. C. Lee, and S.-I. Lee, *Phys. Rev. B* **51**, 3261 (1995).

³ Y. C. Kim, J. R. Thompson, J. G. Ossandon, D. K. Christen, and M. Paranthaman, *Phys. Rev. B* **51**, 11767 (1995).

⁴ R. Puñiak, R. Usami, K. Isawa, and H. Yamauchi, *Phys. Rev. B* **52**, 3756 (1995).

⁵ T. Siegrist, S. M. Zahurak, D. W. Murphy, and R. S. Roth,

Nature **334**, 231 (1988).

⁶ M. G. Smith, A. Manthiram, J. Zhou, J. B. Goodenough, and J. T. Markert, *Nature* **351**, 549 (1991).

⁷ G. Er, S. Kikkawa, F. Kanamaru, Y. Miyamoto, S. Tanaka, M. Sera, M. Sato, Z. Hiroi, M. Takano, and Y. Bando, *Physica C* **196**, 271 (1992).

⁸ J. D. Jorgensen, P. G. Radaelli, D. G. Hinks, J. L. Wagner, S. Kikkawa, G. Er, and F. Kanamaru, *Phys. Rev. B* **47**, 14654 (1993).

- ⁹ N. Ikeda, Z. Hiroi, M. Azuma, M. Takano, Y. Bando, and Y. Takeda, *Physica C* **210**, 367 (1993).
- ¹⁰ D. J. Scalapino, *Phys. Rep.* **250**, 329 (1995).
- ¹¹ D. J. V. Harlingen, *Rev. Mod. Phys.* **67**, 515 (1995).
- ¹² C. C. Tsuei and J. R. Kirtley, *Rev. Mod. Phys.* **72**, 969 (2000).
- ¹³ N. P. Armitage, P. Fournier, and R. L. Greene, *Rev. Mod. Phys.* **82**, 2421 (2010).
- ¹⁴ C. C. Tsuei and J. R. Kirtley, *Phys. Rev. Lett.* **85**, 182 (2000).
- ¹⁵ B. Chesca, K. Ehrhardt, M. Mößle, R. Straub, D. Koelle, R. Kleiner, and A. Tsukada, *Phys. Rev. Lett.* **90**, 057004 (2003).
- ¹⁶ Ariando, D. Darminto, H.-J. H. Smilde, V. Leca, D. H. A. Blank, H. Rogalla, and H. Hilgenkamp, *Phys. Rev. Lett.* **94**, 167001 (2005).
- ¹⁷ C. Gürlich, E. Goldobin, R. Straub, D. Doenitz, Ariando, H.-J. H. Smilde, H. Hilgenkamp, R. Kleiner, and D. Koelle, *Phys. Rev. Lett.* **103**, 067011 (2009).
- ¹⁸ T. Imai, C. P. Slichter, J. L. Cobb, and J. T. Markert, *J. Phys. Chem. Solids* **56**, 1921 (1995).
- ¹⁹ C.-T. Chen, P. Seneor, N.-C. Yeh, R. P. Vasquez, L. D. Bell, C. U. Jung, J. Y. Kim, M.-S. Park, H.-J. Kim, and S.-I. Lee, *Phys. Rev. Lett.* **88**, 227002 (2002).
- ²⁰ G. V. M. Williams, R. Dupree, A. Howes, S. Krämer, H. J. Trodahl, C. U. Jung, M.-S. Park, and S.-I. Lee, *Phys. Rev. B* **65**, 224520 (2002).
- ²¹ V. S. Zapf, N.-C. Yeh, A. D. Beyer, C. R. Hughes, C. H. Mielke, N. Harrison, M. S. Park, K. H. Kim, and S.-I. Lee, *Phys. Rev. B* **71**, 134526 (2005).
- ²² Z. Y. Liu, H. H. Wen, L. Shan, H. P. Yang, X. F. Lu, H. Gao, M.-S. Park, C. U. Jung, and S.-I. Lee, *Europhys. Lett.* **69**, 263 (2005).
- ²³ K. H. Satoh, S. Takeshita, A. Koda, R. Kadono, K. Ishida, S. Pyon, T. Sasagawa, and H. Takagi, *Phys. Rev. B* **77**, 224503 (2008).
- ²⁴ R. Khasanov, A. Shengelaya, A. Maisuradze, D. Di Castro, I. M. Savić, S. Weyeneth, M. S. Park, D. J. Jang, S.-I. Lee, and H. Keller, *Phys. Rev. B* **77**, 184512 (2008).
- ²⁵ J. S. White, E. M. Forgan, M. Laver, P. S. Häfliger, R. Khasanov, R. Cubitt, C. D. Dewhurst, M.-S. Park, D.-J. Jang, H.-G. Lee, et al., *J. Phys.: Condens. Matter* **20**, 104237 (2008).
- ²⁶ M. L. Teague, A. D. Beyer, M. S. Grinolds, S. I. Lee, and N.-C. Yeh, *Europhys. Lett.* **85**, 17004 (2009).
- ²⁷ L. Fruchter, V. Jovanovic, H. Raffy, S. Labdi, F. Bouquet, and Z. Z. Li, *Phys. Rev. B* **82**, 144529 (2010).
- ²⁸ D. A. Wollman, D. J. Van Harlingen, W. C. Lee, D. M. Ginsberg, and A. J. Leggett, *Phys. Rev. Lett.* **71**, 2134 (1993).
- ²⁹ C. C. Tsuei, J. R. Kirtley, C. C. Chi, L. Yu-Jahnes, A. Gupta, T. Shaw, J. Z. Sun, and M. B. Ketchen, *Phys. Rev. Lett.* **73**, 593 (1994).
- ³⁰ R. R. Schulz, B. Chesca, B. Goetz, C. W. Schneider, A. Schmehl, H. Bielefeldt, H. Hilgenkamp, and J. Mannhart, *Appl. Phys. Lett.* **76**, 912 (2000).
- ³¹ B. Chesca, R. R. Schulz, B. Goetz, C. W. Schneider, H. Hilgenkamp, and J. Mannhart, *Phys. Rev. Lett.* **88**, 177003 (2002).
- ³² J. Tomaschko, V. Leca, T. Selistrovski, R. Kleiner, and D. Koelle, *Phys. Rev. B* **84**, 214507 (2011).
- ³³ B. Chesca, *Ann. Phys.* **8**, 511 (1999).
- ³⁴ J. Tomaschko, C. Raisch, V. Leca, T. Chassé, R. Kleiner, and D. Koelle, *Phys. Rev. B* **84**, 064521 (2011).
- ³⁵ J. Tomaschko, V. Leca, T. Selistrovski, S. Diebold, J. Jochum, R. Kleiner, and D. Koelle, *Phys. Rev. B* **85**, 024519 (2012).
- ³⁶ See supplementary material for additional transport data.
- ³⁷ M. B. Ketchen, W. J. Gallagher, A. W. Kleinsasser, S. Murphy, and J. R. Clem, in *SQUID 85, Superconducting Quantum Interference Devices and Their Applications*, Walter de Gruyter, Berlin, New York p. 865 (1985).
- ³⁸ R. Straub, S. Keil, R. Kleiner, and D. Koelle, *Appl. Phys. Lett.* **78**, 3645 (2001).
- ³⁹ D. Koelle, R. Gross, R. Straub, S. Keil, M. Fischer, M. Peschka, R. P. Huebener, and K. Barthel, *Physica C* **332**, 148 (2000).

**Supplementary information to
“Phase-sensitive evidence for $d_{x^2-y^2}$ - pairing symmetry in the
parent-structure high- T_c cuprate superconductor $\text{Sr}_{1-x}\text{La}_x\text{CuO}_2$ ”**

J. Tomaschko,¹ S. Scharinger,¹ V. Leca,^{1,2} J. Nagel,¹ M. Kemmler,¹ T. Selistrovski,¹ D. Koelle,¹ and R. Kleiner^{1,*}

¹*Physikalisches Institut – Experimentalphysik II and Center for Collective Quantum Phenomena in LISA⁺,
Universität Tübingen, Auf der Morgenstelle 14, 72076 Tübingen, Germany*

²*National Institute for Research and Development in Microtechnologies,
Molecular Nanotechnology Laboratory, Erou Iancu Nicolae Str. 126A, RO-077190, Bucharest, Romania*

(Dated: September 23, 2018)

In this supplement we provide additional experimental data for the 0-design SQUID and the π -design SQUID: (I) current voltage (IV) characteristics, (II) voltage V vs. applied field H , (III) symmetry considerations on I_c vs. H , and (IV) a measurement of the current step height caused by the SQUID LC resonances. Most measurements are accompanied by simulations. The model equations are described in section I.

I. CURRENT VOLTAGE CHARACTERISTICS AND MODEL

We start to characterize our devices by discussing their current voltage (IV) characteristics. Fig. S1 (a) shows two IV characteristics of the 0-design SQUID. The magnetic field H , applied perpendicularly to the substrate plane, was adjusted such that the SQUID’s critical current was at its first (counted from zero applied field) maximum (black circles, $\mu_0 H = 0.01 \mu\text{T}$) or at its first minimum (grey circles, $\mu_0 H = 0.1 \mu\text{T}$). In both cases the IV characteristics were nonhysteretic. They can be very well fitted by numerically calculated curves, solving the SQUID Langevin equations¹, extended by taking the nonzero junction width into account. The model assumes that the Josephson junctions can be described by the resistively and capacitively shunted junction model^{2,3}. We have assumed further, that a fraction f_J of the flux Φ through the SQUID loop is homogeneously coupled into the junctions, causing a linear increase of the Josephson phase differences γ_k ($k = 1, 2$) inside the junctions. This contribution has been integrated out analytically, yielding a sinc function for the critical current I_0 vs. Φ for each junction.

The normalized currents $i = I/I_0$ through the junctions are given by

$$\frac{i}{2} \pm j = \beta_c \ddot{\gamma}_k + \dot{\gamma}_k + i_c(\Phi) \sin(\gamma_k) + i_{N,k} \quad (1)$$

where $k = 1, 2$ labels the two Josephson junctions. I_0 is the amplitude of the Josephson current, $j = J/I_0$ is the normalized circulating current in the SQUID loop and ‘ \pm ’ refers to junctions 1 and 2, respectively. $\beta_c = 2\pi I_0 R^2 C/\Phi_0$ is the Stewart-McCumber parameter. Φ_0 is the flux quantum and R and C , re-

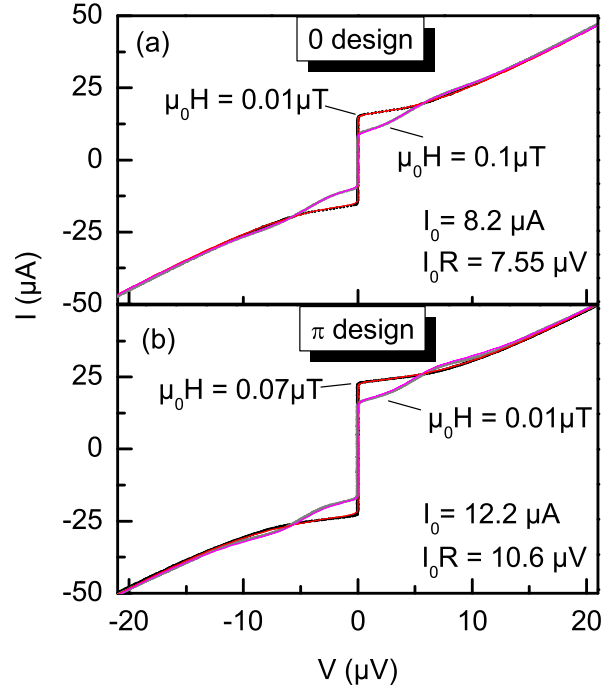


FIG. S1: (Color online) Current voltage (IV) characteristics of (a) the 0-design SQUID and (b) the π -design SQUID. Each graph contains two measured curves and two calculated curves. Measurements were taken at, respectively, maximum (black circles) and minimum (grey circles) critical current. Calculated curves were obtained by numerically solving the SQUID Langevin equations, extended by taking the nonzero junction width into account, for (a) a 0 SQUID at flux $\Phi = 0$ (red line) and $\Phi = \Phi_0/2$ (magenta line), and (b) for a π SQUID at flux $\Phi = \Phi_0/2$ (red line) and $\Phi = \Phi_0$ (magenta line). Model parameters in (a) are $\beta_c = 0.5$, $\beta_L = 1.4$, $\Gamma = 0.022$, $a_L = 0.05$ and $f_J = 0.128$. By matching abscissa and ordinate of the measured and calculated curves one obtains $I_0 = 8.2 \mu\text{A}$ and $I_0 R = 7.55 \mu\text{V}$. Model parameters in (b) are $\beta_c = 0.7$, $\beta_L = 2.2$, $\Gamma = 0.0147$, $a_L = 0.05$, $f_J = 0.12$, $I_0 = 12.2 \mu\text{A}$ and $I_0 R = 10.6 \mu\text{V}$. The same set of parameters was used for all curves discussed in this paper.

spectively, denote junction resistance and capacitance. γ_k is the Josephson phase difference across junction k and the dots denote derivative with respect to time. The flux dependent quantity $i_c(\Phi)$ is given by $i_c(\Phi) =$

$\sin(\pi f_J \Phi / \Phi_0) / [\pi f_J \Phi / \Phi_0]$. The normalized noise current $i_{N,k}$ has a spectral power density 4Γ , with $\Gamma = 2\pi k_B T / I_0 \Phi_0$. The above equations assumed that the junction parameters β_c and $i_c(\Phi)$ are the same for both junctions. If junction k is a π junction, a phase π is to be added to γ_k .

The two phases γ_k are related by

$$\gamma_2 - \gamma_1 = 2\pi\Phi/\Phi_0 + \pi\beta_L(j + a_L i) \quad (2)$$

where $\beta_L = 2I_0 L / \Phi_0$. $L = L_1 + L_2$, where L_1 and L_2 are the inductances of the two SQUID arms, related to the inductance asymmetry a_L via $L_k = L(1 \pm a_L)/2$.

From Eqs. (1) and (2) one obtains the normalized voltage $v = V/I_0 R$, and thus current voltage characteristics, critical current vs. flux etc., by taking the time average of $(\dot{\gamma}_1 + \dot{\gamma}_2)/2$. A consistent set of model parameters can be obtained by analyzing IV characteristics at maximum and minimum I_c , plus I_c vs. H .

The calculated IV characteristics in Fig. S1 (a) are for $\beta_c = 0.5$, $\beta_L = 1.4$, $\Gamma = 0.022$, $a_L = 0.05$ and $f_J = 0.128$ (the latter two numbers are actually determined from I_c vs. H data). In dimensioned units one finds $I_0 = 8.2 \mu\text{A}$ and $I_0 R = 7.55 \mu\text{V}$, $R = 0.92 \Omega$, $L = 177 \text{pH}$, $C = 24 \text{pF}$. These are reasonable numbers for our SQUIDs. In the $\mu_0 H = 0.1 \mu\text{T}$ curve of Fig. S1 (a) one also notices a hump for $6 \mu\text{V} < V < 10 \mu\text{V}$. This is a LC resonance, which becomes maximally excited when the supercurrents across the two junctions oscillate out-of-phase¹.

Two IV characteristics for the π -design SQUID are shown in Fig. S1 (b). One first notices that the first I_c maximum (black circles) was obtained at a relatively large field, $0.07 \mu\text{T}$. By contrast, at $\mu_0 H = 0.01 \mu\text{T}$, I_c had a minimum (grey circles). Simulating these curves (red line for $\mu_0 H = 0.07 \mu\text{T}$ and magenta line for $\mu_0 H = 0.01 \mu\text{T}$) we have assumed that junction 2 is a π junction and further used the parameters $\beta_c = 0.7$, $\beta_L = 2.2$, $\Gamma = 0.0147$, $a_L = 0.05$, $f_J = 0.12$, $I_0 = 12.2 \mu\text{A}$, $I_0 R = 10.6 \mu\text{V}$, $R = 0.87 \Omega$, $C = 25 \text{pF}$, $L = 187 \text{pH}$, which are not very different from the reference SQUID.

II. VOLTAGE VS. APPLIED FIELD

Fig. S2 shows measured [(a), (c)] and calculated [(b),(d)] patterns V vs. H for the 0-design SQUID [(a), (b)] and the π -design SQUID [(c),(d)]. The data were obtained in the same run as the IV characteristics of Fig. S1 and the I_c vs. H data (Fig. 2 of the main paper). In the measurements the current I across the 0-design SQUID has been increased (decreased) from 0 in steps of $1 \mu\text{A}$ up to $\pm 28 \mu\text{A}$. For the π -design SQUID the step width was $0.98 \mu\text{A}$, with a maximum current $\pm 39.5 \mu\text{A}$. Measured data for the 0-design SQUID, cf. Fig. S2 (a), are smooth and well reproduced by the calculated patterns [Fig. S2 (b)]. Note that for voltages below $|V| \approx 5 \mu\text{V}$ the $|V|$ vs. H minima are located near $H = 0$ (modulo modulation period), while for $|V| > 5 \mu\text{V}$ one finds a

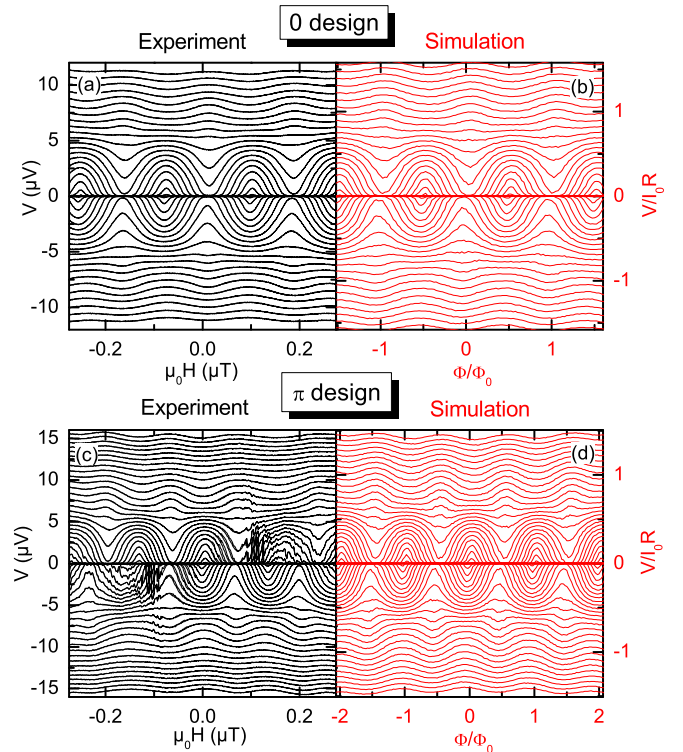
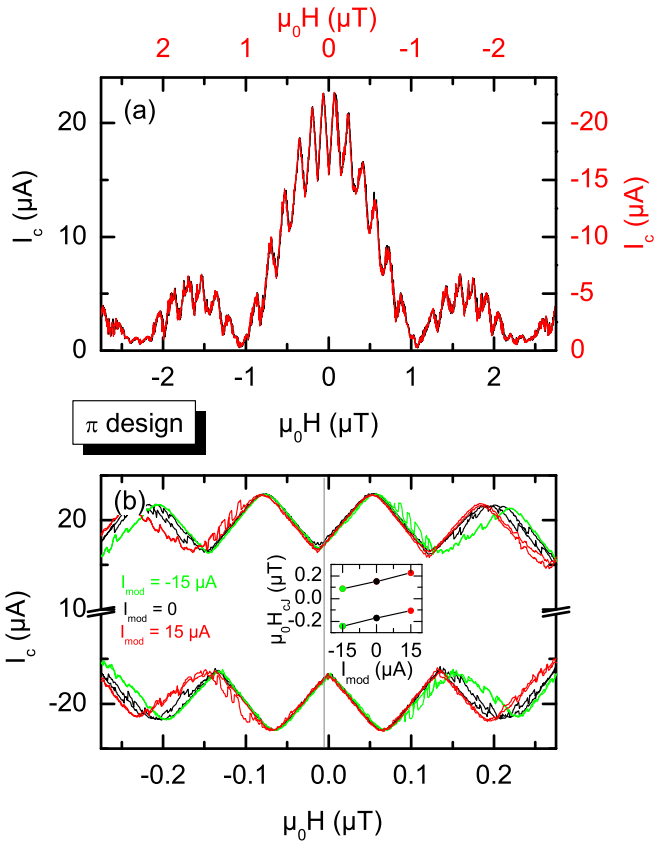


FIG. S2: (Color online) Measured V vs. H for (a) the 0-design SQUID and (c) the π -design SQUID together with numerically calculated curves for (b) the 0-design SQUID and (d) the π -design SQUID. The current I across the 0-design SQUID has been increased (decreased) from 0 in steps of $1 \mu\text{A}$ up to $\pm 28 \mu\text{A}$. For the π -design SQUID the step width was $0.98 \mu\text{A}$, with a maximum current $\pm 39.5 \mu\text{A}$.

maximum here. This is due to the LC resonance which is also visible in Fig. S1 (a). Further, the $|V|$ vs. H maxima appear (modulo modulation period) near $\mu_0 H = 0.995 \mu\text{T}$ and are slightly shifted with respect to the origin of the ordinate. This shift, which is due to the small inductance asymmetry, was seen already in I_c vs. H . Otherwise, the device behaves as it can be expected for a 0 SQUID. In the experimental data for the π -design SQUID one observes similar features, but shifted by a half period with respect to the π -design SQUID. As in I_c vs. H , jumps appear in the second SQUID modulation period at positive H at positive V and at negative H at negative V . This point symmetry was already visible in the I_c vs. H data. Apart from these jumps, V vs. H is reasonably well reproduced by simulations, cf. Fig. S2 (b).

III. CRITICAL CURRENT VS. APPLIED FIELD: SYMMETRY CONSIDERATIONS

In Fig. S3 (a) we further demonstrate point symmetry by plotting the negative I_c as $-I_c$ vs. $-\mu_0 H$ (red line)



on top of I_c vs. $\mu_0 H$ for the positive I_c (black line). The curves are basically indistinguishable.

The point symmetry gives some hint on the properties of the trapped flux. First, if Abrikosov vortices or Josephson fluxons were trapped permanently one would at most expect a symmetry with respect to a change $I \leftrightarrow -I$. The point symmetry implies that also the *polarity* of the trapped flux changes by reversing the magnetic field. The fact that the I_c jumps exhibit almost no hysteresis further implies that almost no pinning is present. All this, together with the observation that jumps in I_c vs. H are absent for the 0-design SQUID, supports the suspicion that Josephson fluxons enter and leave GBJ 1. The change in polarity of the trapped flux with applied field implies that *no fluxons* are present at low fields, allowing to interpret our data in terms of a π SQUID and thus in favor of a $d_{x^2-y^2}$ -wave order parameter symmetry.

The I_c jumps in Fig. 2 (b) of the main paper were strongly asymmetric with respect to the applied field. For positive current the first I_c jumps occurred at the

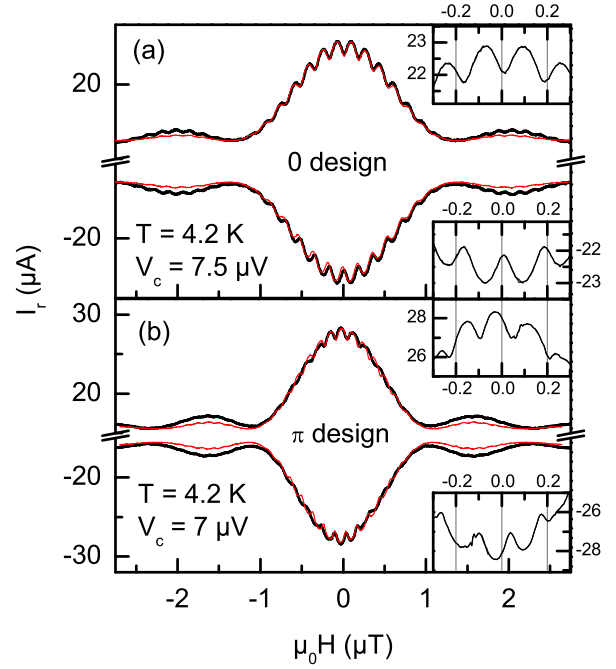


FIG. S4: (Color online) Resonance current I_r vs. applied field for (a) the 0-design SQUID and (b) the π -design SQUID (black curves), together with the corresponding simulated curves (red lines). Insets show I_r vs. H at expanded current and field scales.

penetration fields $\mu_0 H_{\text{cJ}} = +0.09 \mu\text{T}$ and at $-0.24 \mu\text{T}$. At negative current they were observable at $\mu_0 H_{\text{cJ}} = -0.09 \mu\text{T}$ and at $+0.24 \mu\text{T}$. This asymmetry was different in different cooldowns and seemed to depend on the residual field. In fact, screening currents across GBJ 1 will change the surface barrier for fluxon entry, making H_{cJ} asymmetric. Fig. S3 (b) shows results from another cooldown where the jumps occurred almost symmetrically with respect to H (black line). In this graph we also show two measurements, where we applied an additional modulation current I_{mod} across GBJ 1, cf. Fig. 1 in the main paper. Depending on the polarity of this current its effect was to linearly shift the appearance of the I_c jumps, *i.e.* H_{cJ} , to higher (lower) values for positive (negative) values of I_{mod} . This shift did not depend on the sign of I . I_{mod} exerts a Lorentz force on the fluxons. For $I_{\text{mod}} > 0$ fluxons appearing at $H > 0$ are repelled from the SQUID, increasing the switching fields for both polarities of I . The force on antifluxons appearing at $H < 0$ points inward, *i.e.*, the switching field decreases. For $I_{\text{mod}} < 0$ the forces on fluxons and antifluxons are opposite. Thus, the shifts of the I_c jumps are fully compatible with the notion of (anti)fluxons having entered GBJ 1.

IV. *LC* RESONANCES

We finally address in more detail the resonance feature which appeared as a hump in the *IV* characteristics at $\mu_0 H = 0.1 \mu\text{T}$ for the 0-design SQUID and at $\mu_0 H = 0.01 \mu\text{T}$ for the π -design SQUID. In V vs. H the resonance appeared as a phase shift of a half period in the SQUID modulation. These effects are due to resonantly excited circulation currents across the SQUID loop and occur when the Josephson currents across the two junctions acquire an out-of phase component. Maximum excitation occurs when the Josephson currents oscillate maximally out-of-phase. For a 0 SQUID one thus expects the strongest effect for a half flux quantum applied to the

junction, for a π SQUID it should be strongest at integer multiples of Φ_0 ⁴. To investigate the *LC* resonance vs. applied field H we have determined the “resonance current” I_r across the SQUIDs by using a voltage criterion V_c which corresponds to the center of the hump feature in the *IV* characteristics (7.5 μV for the 0-design SQUID and 7 μV for the π -design SQUID).

Fig. S4 (a) shows I_r vs. H for the 0-design SQUID (black line) together with a simulated curve (red line). Apart from a slight offset due to residual fields the minimum in I_r is at zero field both for negative and positive values of I_r . By contrast, for the π -design SQUID one finds (except for an offset) a maximum of I_r near zero field, again indicative of a π SQUID.

* Electronic address: kleiner@uni-tuebingen.de

¹ J. Clarke and A. I. Braginski, *The SQUID Handbook*, vol. 1 (WILEY-VCH Verlag GmbH & Co. KGaA, Weinheim, Germany, 2004).

² W. C. Stewart, *Appl. Phys. Lett.* **12**, 277 (1968).

³ D. E. McCumber, *J. Appl. Phys.* **39**, 3113 (1968).

⁴ B. Chesca, R. R. Schulz, B. Goetz, C. W. Schneider, H. Hilgenkamp, and J. Mannhart, *Phys. Rev. Lett.* **88**, 177003 (2002).